Title

Three-dimensional corner eddies in Stokes flow

Journal

Fluid Dynamics Research, 46(1)

ISSN

0169-5983

Authors

Davis, Anthony MJ
Smith, Stefan G Llewellyn

Publication Date

2014-02-01

DOI

10.1088/0169-5983/46/1/015509

Peer reviewed

Three-dimensional corner eddies in Stokes flow

Anthony M J Davis and Stefan G Llewellyn Smith

Department of Mechanical and Aerospace Engineering, Jacobs School of Engineering, UCSD, 9500 Gilman Drive, La Jolla CA 92093-0411, USA

E-mail: amdavis@ucsd.edu, sgls@ucsd.edu

Abstract. Vortices exist in wedge-shaped corners in Stokes flow. In seeking an analogous eigensolution structure in three dimensions, an analytic construction is derived for a rectangular corner. This restriction mirrors the only corner type for which computed streamlines are available for comparison and explanation. The dominant eigenvalue is complex, giving rise to localized eddies. Hence trapped fluid is predicted near the corner.

1. Introduction

Dean and Montagnon (1949) showed that complex eigenvalues exist for steady viscous self-similar flow in a corner of angle less than 146°. Moffatt (1964) inferred the existence of a sequence of vortices that now bear his name, in two-dimensional Stokes flow. Wakiya (1976)), followed by Liu and Joseph (1978), showed that the corresponding axisymmetric vortices can exist within a cone and Malhotra et al. (2005) added the two cone geometry. By means of asymptotic methods, the presence of such vortices was identified in cylinder/plane (Davis and O'Neill 1977), two-sphere (Davis et al. 1976) and wall-driven rectangular cavity (Meleshko 1996) flows. However, asymmetric three-dimensional flows are unlikely to exhibit vortices because the boundaries lack the confining effect needed to trap the creeping flow.

The quest for eddies in a genuinely three-dimensional flow has been pursued by considering suitably chosen examples. Hills and Moffatt (2000) analysed the asymptotic behavior of the flow near the edge formed by two fixed rectangular fins placed in a rotating cone and identified a sequence of eddies whose streamlines lie on concentric spheres, centered at the cone's vertex. Gomilko et al. (2003) displayed eddies generated by boundary-driven flows in a trihedral rectangular corner. Further sets of computed eddy streamlines in such corners are given by Shankar and Deshpande (2000) and Shankar (2007), whose lid-driven cavity flows also feature the self-similar flow in a right-angled corner that is analyzed below. Leriche and Labrosse (2011) find eigenmodes for Stokes flow in a cubical cavity and discuss the flow in corners. Guglielmini et al. (2011) have shown helical-like structures, that is, the streamlines are not closed, in three-dimensional pressure-driven confined channel flow around corners. Their results, which

depend on the channel's aspect ratio, have been confirmed experimentally by Sznitman et al. (2012). Mustakis and Kim (1998) calculate solutions outside a cube and examine the solution near a vertex, but do not investigate the presence of eddies.

The three-dimensional flows mentioned above are, with one exception, driven by the motion of boundaries. The aim here is to understand the flow in a corner bounded by planes at rest, driven by some motion in the far field, as at the base of the lid-driven cavity, to see if eddies develop. The first step towards extending the wedge results of Dean and Montagnon (1949) and Moffatt (1964) to a tetrahedral corner was recently presented by Scott (2013), who showed numerically that the flow field in the slowest decaying mode has symmetric and antisymmetric components. This, possibly unexpected, result is yet another example of the rich variety of three-dimensional flows. The approach adopted below is essentially analytical, with numerical work appearing at a late stage.

2. Self similar flow in a right-angled corner

Consider the corner, $r > 0$, $0 < \theta < \pi/2$, $0 < \phi < \pi/2$, in terms of spherical polar coordinates (r, θ, ϕ). In Stokes flow, the dimensionless velocity and pressure fields are governed by

$$\nabla \cdot \mathbf{v} = 0, \qquad \nabla^2 \mathbf{v} = \nabla p. \tag{1}$$

With $\mathbf{v} = u\hat{\boldsymbol{r}} + v\hat{\boldsymbol{\theta}} + w\hat{\boldsymbol{\phi}}$, the continuity equation suggests a similarity solution of the form

$$u = r^\lambda U, \qquad (v, w) = r^\lambda (V, W) \sin\theta, \qquad p = r^{\lambda-1} P. \tag{2}$$

2.1. Solutions with azimuthal trigonometric dependence

Set $\sigma = \cos\theta$ and seek solutions

$$(U, V, P) = [f(\sigma), g(\sigma), k(\sigma)] \sin\nu\phi, \qquad W = h(\sigma)\cos\nu\phi. \tag{3}$$

Then $\nabla^2 p = 0$ implies that

$$k = A P^\nu_{\lambda-1}(\sigma), \tag{4}$$

for some constant A.

A suitable velocity representation in spherical polar coordinates, which proves superior to Lamb's general solution, is

$$\mathbf{v} = \nabla \times \nabla \times (\mathbf{r}\Psi) + \nabla \times (\mathbf{r}\chi), \qquad p = (1 + \mathbf{r} \cdot \nabla)\nabla^2 \Psi, \tag{5}$$

where $\nabla^4 \Psi = 0 = \nabla^2 \chi$ (Davis 1983). Then

$$\nabla \times [\mathbf{r} r^\lambda P^\nu_\lambda(\sigma)\cos\nu\phi] = r^\lambda \left[-\frac{\nu}{\sqrt{1-\sigma^2}} P^\nu_\lambda(\sigma)\sin\nu\phi\, \hat{\boldsymbol{\theta}} + \sqrt{1-\sigma^2}\frac{\mathrm{d}P^\nu_\lambda}{\mathrm{d}\sigma}\cos\nu\phi\, \hat{\boldsymbol{\phi}} \right], \tag{6}$$

which yields a solution of type (3) with

$$h^{III} = \frac{\mathrm{d}P^\nu_\lambda}{\mathrm{d}\sigma}, \qquad g^{III} = -\frac{\nu P^\nu_\lambda}{1-\sigma^2}, \qquad f^{III} = 0 = k^{III}. \tag{7}$$

Since

$$\nabla \times \nabla \times (\mathbf{r}\Psi) = \nabla[\Psi + \mathbf{r} \cdot \nabla\Psi] - \mathbf{r}\nabla^2\Psi \tag{8}$$

and

$$\nabla \times \nabla \times [\mathbf{r} r^{\lambda+1} P^\nu_{\lambda+1}(\sigma) \sin\nu\phi] = r^\lambda(\lambda+2)\left[(\lambda+1)P^\nu_{\lambda+1}\sin\nu\phi\,\hat{\boldsymbol{r}}\right.$$
$$\left. -\sqrt{1-\sigma^2}\frac{\mathrm{d}P^\nu_{\lambda+1}}{\mathrm{d}\sigma}\sin\nu\phi\,\hat{\boldsymbol{\theta}} + \frac{\nu}{\sqrt{1-\sigma^2}}P^\nu_{\lambda+1}\cos\nu\phi\,\hat{\boldsymbol{\phi}}\right], \tag{9}$$

a solution of type (3) is given by

$$f^{II} = (\lambda+1)P^\nu_{\lambda+1}, \quad g^{II} = -\frac{\mathrm{d}P^\nu_{\lambda+1}}{\mathrm{d}\sigma}, \quad h^{II} = \frac{\nu P^\nu_{\lambda+1}}{1-\sigma^2}, \quad k^{II} = 0. \tag{10}$$

Similarly, $\nabla \times \nabla \times [\mathbf{r} r^{\lambda+1} P^\nu_{\lambda-1}(\sigma)\sin\nu\phi]$ yields a third solution with

$$f^I = \frac{\lambda(\lambda-1)}{\lambda+2}P^\nu_{\lambda-1}, \quad g^I = -\frac{\mathrm{d}P^\nu_{\lambda-1}}{\mathrm{d}\sigma}, \quad h^I = \frac{\nu P^\nu_{\lambda-1}}{1-\sigma^2}, \quad k^I = \frac{2\lambda(2\lambda+1)}{\lambda+2}P^\nu_{\lambda-1}. \tag{11}$$

The only non-vanishing k is in agreement with (4). Except for the rescaling of I, these independent solutions are those derived from Lamb's general solution by Gomilko et al. (2003). For $0 \le \sigma \le 1$, a useful formula, given by Gradshteyn and Ryzhik (2000, 8.704), is

$$P^\nu_\lambda(\sigma) = P^\nu_{-\lambda-1}(\sigma) = \frac{1}{\Gamma(1-\nu)}\left(\frac{1+\sigma}{1-\sigma}\right)^{\nu/2} F\left(-\lambda, \lambda+1; 1-\nu; \frac{1-\sigma}{2}\right). \tag{12}$$

Both the power of r and the functions in solution I imply that Re $\lambda \ge 1/2$ may be assumed henceforth, since complex conjugate eigenvalues are anticipated. A particular value of (12), given by Gradshteyn and Ryzhik (2000, 8.756.1), is

$$P^{-2m}_\lambda(0) = \frac{2^{-2m}\sqrt{\pi}}{\Gamma(m+1+\frac{\lambda}{2})\Gamma(m-\frac{\lambda-1}{2})}, \tag{13}$$

which vanishes if and only if λ is an odd integer $\ge 2m+1$ and is consistent with Gradshteyn and Ryzhik (2000, 8.736.1)

$$P^{-2m}_\lambda(\sigma) = \frac{\Gamma(\lambda-2m+1)}{\Gamma(\lambda+2m+1)}P^{2m}_\lambda(\sigma). \tag{14}$$

2.2. Imposition of no-slip

If $\nu = -2m$ in (3), then $(U, V) = (0, 0)$ at $\phi = 0, \pi/2$, that is, the tangential components vanish at these two walls. For $(U, W) = (0, 0)$ at $\theta = \pi/2$, (7, 10, 11) are suitably combined to obtain, for mode $m \ge 1$,

$$U_m = \left[\frac{P^{-2m}_{\lambda-1}(\sigma)}{P^{-2m}_{\lambda-1}(0)} - \frac{P^{-2m}_{\lambda+1}(\sigma)}{P^{-2m}_{\lambda+1}(0)}\right]\sin 2m\phi, \tag{15}$$

$$W_m = \left[\frac{2m(\lambda+2)P^{-2m}_{\lambda-1}(\sigma)}{\lambda(\lambda-1)(1-\sigma^2)P^{-2m}_{\lambda-1}(0)} - \frac{2mP^{-2m}_{\lambda+1}(\sigma)}{(\lambda+1)(1-\sigma^2)P^{-2m}_{\lambda+1}(0)}\right.$$
$$\left. -C_m\frac{\mathrm{d}P^{-2m}_\lambda/\mathrm{d}\sigma(\sigma)}{\mathrm{d}P^{-2m}_\lambda/\mathrm{d}\sigma(0)}\right]\cos 2m\phi, \tag{16}$$

where

$$C_m = \frac{2m(\lambda+2)}{\lambda(\lambda-1)} - \frac{2m}{\lambda+1}. \tag{17}$$

Use of the recurrence relations

$$(2\lambda+1)\sigma P_\lambda^\nu = (\lambda+\nu)P_{\lambda-1}^\nu + (\lambda+1-\nu)P_{\lambda+1}^\nu, \tag{18}$$

$$(1-\sigma^2)\frac{d}{d\sigma}P_\lambda^\nu = \frac{1}{2\lambda+1}\left[(\lambda+1)(\lambda+\nu)P_{\lambda-1}^\nu - \lambda(\lambda+1-\nu)P_{\lambda+1}^\nu\right], \tag{19}$$

yields the much simpler form

$$W_m = \frac{2m}{\lambda-1}\left[\frac{P_{\lambda-1}^{-2m}(\sigma)}{P_{\lambda-1}^{-2m}(0)} - \frac{P_{\lambda+1}^{-2m}(\sigma)}{P_{\lambda+1}^{-2m}(0)}\right]\frac{\cos 2m\phi}{1-\sigma^2}. \tag{20}$$

Evidently there is no role for the $m=0$ mode. The corresponding $\hat{\boldsymbol{\theta}}$-component of (3) is given by

$$V_m = \left[-\frac{(\lambda+2)\mathrm{d}P_{\lambda-1}^{-2m}/\mathrm{d}\sigma(\sigma)}{\lambda(\lambda-1)P_{\lambda-1}^{-2m}(0)} + \frac{\mathrm{d}P_{\lambda+1}^{-2m}/\mathrm{d}\sigma(\sigma)}{(\lambda+1)P_{\lambda+1}^{-2m}(0)} + C_m\frac{2mP_\lambda^{-2m}(\sigma)}{(1-\sigma^2)\mathrm{d}P_\lambda^{-2m}/\mathrm{d}\sigma(0)}\right]\sin 2m\phi, \tag{21}$$

which can be similarly reduced to

$$V_m = \left[\left(\frac{2\lambda+1}{\lambda-1}\right)P_\lambda^{-2m}(\sigma) - \frac{(\lambda+2)(\lambda-2m)}{\lambda-1}\sigma P_{\lambda-1}^{-2m}(\sigma) + (\lambda+2m+1)\sigma P_{\lambda+1}^{-2m}(\sigma)\right]\frac{\sin 2m\phi}{(1-\sigma^2)\mathrm{d}P_\lambda^{-2m}/\mathrm{d}\sigma(0)}. \tag{22}$$

In particular,

$$(V_m)_{\sigma=0} = \left(\frac{2\lambda+1}{\lambda-1}\right)\frac{P_\lambda^{-2m}(0)}{\mathrm{d}P_\lambda^{-2m}/\mathrm{d}\sigma(0)}\sin 2m\phi \tag{23}$$

which is required below.

We set

$$\mathbf{v} = r^\lambda \sum_{i=1}^{3}\sum_{m=1}^{\infty} F_m^{(i)}\left[U_m(\sigma^{(i)},\phi^{(i)})\hat{\boldsymbol{r}} + [V_m(\sigma^{(i)},\phi^{(i)})\hat{\boldsymbol{\theta}}^{(i)} + W_m(\sigma^{(i)},\phi^{(i)})\hat{\boldsymbol{\phi}}^{(i)}]\sin\theta^{(i)}\right], \tag{24}$$

where $(r,\theta^{(i)},\phi^{(i)})$ $(i=1,2,3)$ are the three sets of spherical polar coordinates defined by Gomilko et al. (2003), with the $\theta^{(1)}=0$, $\theta^{(2)}=0$, $\theta^{(3)}=0$ axes coincident with the positive z,x,y-axes respectively (see Figure 1). At the three walls, all tangential velocities are zero. On $z=0$ ($\theta^{(1)}=\pi/2$, $\sigma^{(1)}=0$), only the $\hat{\theta}^{(1)}$-component at $\theta^{(1)}=\pi/2$ ($\sigma^{(1)}=0$) is required, while

$$\theta^{(2)}=\phi^{(1)},\ \ \phi^{(2)}=0,\ \ \theta^{(3)}=\pi/2-\phi^{(1)},\ \ \phi^{(3)}=\pi/2,\ \ \hat{\boldsymbol{\theta}}^{(1)}=-\hat{\boldsymbol{\phi}}^{(2)},\ \ \hat{\boldsymbol{\theta}}^{(1)}=\hat{\boldsymbol{\phi}}^{(3)}. \tag{25}$$

Thus, from (24),

$$(\mathbf{v})_{\sigma^{(1)}=0} = r^\lambda\hat{\boldsymbol{\theta}}^{(1)}\sum_{m=1}^{\infty}\left[F_m^{(1)}V_m(0,\phi^{(1)}) - F_m^{(2)}W_m(\cos\phi^{(1)},0)\sin\phi^{(1)} + F_m^{(3)}W_m(\sin\phi^{(1)},\pi/2)\cos\phi^{(1)}\right], \tag{26}$$

whose required vanishing gives, on substitution of (20, 23),

$$\sum_{m=1}^{\infty}\left\{F_m^{(1)}\left(\frac{2\lambda+1}{\lambda-1}\right)\frac{P_\lambda^{-2m}(0)}{\mathrm{d}P_\lambda^{-2m}/\mathrm{d}\sigma(0)}\sin 2m\phi\right.$$
$$-F_m^{(2)}\frac{2m}{\lambda-1}\left[\frac{P_{\lambda-1}^{-2m}(\cos\phi)}{P_{\lambda-1}^{-2m}(0)}-\frac{P_{\lambda+1}^{-2m}(\cos\phi)}{P_{\lambda+1}^{-2m}(0)}\right]\frac{1}{\sin\phi}$$
$$\left.+F_m^{(3)}\frac{2m}{\lambda-1}\left[\frac{P_{\lambda-1}^{-2m}(\sin\phi)}{P_{\lambda-1}^{-2m}(0)}-\frac{P_{\lambda+1}^{-2m}(\sin\phi)}{P_{\lambda+1}^{-2m}(0)}\right]\frac{(-1)^m}{\cos\phi}\right\}=0. \tag{27}$$

Noting that

$$\int_0^{\pi/2} f(\sin\phi)\sin 2n\phi\,\mathrm{d}\phi=(-1)^{n+1}\int_0^{\pi/2} f(\cos\phi)\sin 2n\phi\,\mathrm{d}\phi, \tag{28}$$

the Fourier components of (27) yield, for $n\geq 1$,

$$\sum_{m=1}^{\infty}\left\{F_m^{(1)}(2\lambda+1)\delta_{mn}\frac{P_\lambda^{-2m}(0)}{\mathrm{d}P_\lambda^{-2m}/\mathrm{d}\sigma(0)}-\frac{8m}{\pi}[F_m^{(2)}+(-1)^{m+n}F_m^{(3)}]\times\right.$$
$$\left.\int_0^{\pi/2}\left[\frac{P_{\lambda-1}^{-2m}(\cos\phi)}{P_{\lambda-1}^{-2m}(0)}-\frac{P_{\lambda+1}^{-2m}(\cos\phi)}{P_{\lambda+1}^{-2m}(0)}\right]\frac{\sin 2n\phi}{\sin\phi}d\phi\right\}=0. \tag{29}$$

Corresponding equations on the other bounding planes $x=0$ and $y=0$ are obtained by cyclic permutation of the index i. Thus the general system has three sets of equations of type (29). However, disjoint subsets are available. Solutions with rotational symmetry, that is, invariant under the permutations $x\to y\to z\to x$ exist with $F_m^{(1)}=F_m^{(2)}=F_m^{(3)}$. Inspection of (15, 20) shows that even and odd values of m yield modes that are respectively antisymmetric and symmetric with respect to the midplane $\phi=\pi/4$. Evidently the single system then splits into disjoint systems for the even and odd coefficients F_m. As observed by Scott (2013), there exist modes that are superpositions of antisymmetric and symmetric velocity fields. Reference to (24) shows that these solutions have the forms

$$\mathbf{v}=r^\lambda\sum_{q=1}^{\infty}F_{2q}\left[U_{2q}(\sigma^{(1)},\phi^{(1)})\hat{\boldsymbol{r}}+[V_{2q}(\sigma^{(1)},\phi^{(1)})\hat{\boldsymbol{\theta}}^{(1)}+W_{2q}(\sigma^{(1)},\phi^{(1)})\hat{\boldsymbol{\phi}}^{(1)}]\sin\theta^{(1)}\right]$$
$$+r^\lambda\sum_{i=2}^{3}\sum_{q=1}^{\infty}F_{2q-1}\left[U_{2q-1}(\sigma^{(i)},\phi^{(i)})\hat{\boldsymbol{r}}\right.$$
$$\left.+[V_{2q-1}(\sigma^{(i)},\phi^{(i)})\hat{\boldsymbol{\theta}}^{(i)}+W_{2q-1}(\sigma^{(i)},\phi^{(i)})\hat{\boldsymbol{\phi}}^{(i)}]\sin\theta^{(i)}\right], \tag{30}$$

and similarly with odd and even coefficients and velocities interchanged. Thus, in either case, two systems of type (29) are obtained.

2.3. Phantom real eigenvalues

The above analysis assumes that $P_{\lambda\pm1}^{-2m}(0)\neq 0$ and $\mathrm{d}P_\lambda^{-2m}/\mathrm{d}\sigma(0)\neq 0$ for $m>0$. On noting that

$$P_{2k-1}^{2m}(\sigma)=0\ (m\geq k),\qquad P_{2k-1}^{2m}(0)=0\ (m<k), \tag{31}$$

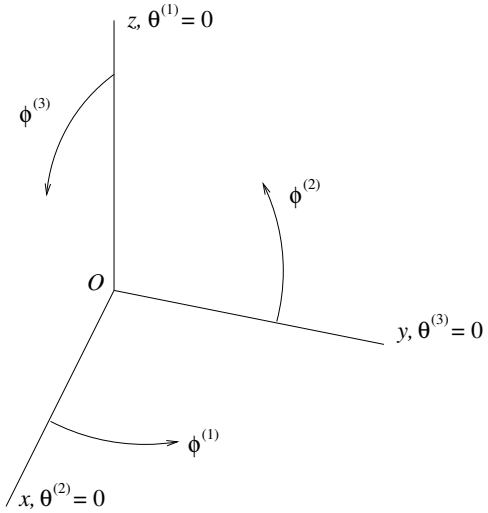

Figure 1. Geometry of the problem and coordinate systems after Gomilko et al. (2003).

$$P^{2m}_{2k+1}(\sigma) = 0 \ (m > k), \qquad P^{2m}_{2k+1}(0) = 0 \ (m \leq k), \tag{32}$$

$$\frac{\mathrm{d}P^{2m}_{2k}}{\mathrm{d}\sigma}(\sigma) = 0 \ (m > k), \qquad \frac{\mathrm{d}P^{2m}_{2k-1}}{\mathrm{d}\sigma}(0) = 0 \ (m \leq k), \tag{33}$$

and that contributions to the normal velocity in (24) in the rotationally symmetric modes are of type $r^\lambda \times$

$$\begin{aligned} &V_m(0,\phi) - W_m(\cos\phi, 0)\sin\phi + W_m(\sin\phi, \pi/2)\cos\phi \\ &= -g(0)\sin 2m\phi - h(\cos\phi)\sin\phi + (-1)^m h(\sin\phi)\cos\phi, \end{aligned} \tag{34}$$

it is found that, in general, $\lambda = 2k$ (with $k \geq 1$) yields $(3k-1)$ linear combinations of the k functions $\sin 2m\phi$ with $1 \leq m \leq k$, and thus is an eigenvalue of multiplicity $(2k-1)$. Evaluation of the associated velocity fields requires that a component of (24) be expressed in Cartesian form, giving

$$v_x(x,y,z)\hat{\boldsymbol{x}} + v_y(x,y,z)\hat{\boldsymbol{y}} + v_z(x,y,z)\hat{\boldsymbol{z}}, \tag{35}$$

whence, for example, the $\hat{\boldsymbol{z}}$-component of (24) is $v_x(z,x,y) + v_y(y,z,x) + v_z(x,y,z)$. This is found to be zero, algebraically for the $\lambda = 2$ field and three $\lambda = 4$ fields, and numerically for the five $\lambda = 6$ fields. The complexity increases significantly with λ and a similar result for arbitrary λ is here stated empirically.

3. Numerical Determination of Eigenvalues

A numerical solution of the infinite linear system (29) is obtained by truncating at finite $m = M$. The resulting finite homogeneous system has a solution if the determinant of the matrix multiplying the vector $(F^{(1)}_1, F^{(2)}_1, F^{(3)}_1, \ldots, F^{(1)}_M, F^{(2)}_M, F^{(3)}_M)^T$ has zero determinant.

The four lowest eigenvalues (ordered by their real part) are 3.264 ± 1.1616i, 5.2942 ± 1.645i, 5.3538 ± 1.2874i and 5.380608242, accurate to the digits given. These results were obtained using $M = 256$, while the integrals were computed using the trapezoidal rule with 255 interior points. The values of the eigenvalues are the same as those found by Scott (2013). The first two eigenvalues are double, corresponding to a symmetric and an antisymmetric mode about the midplane $\phi = \pi/4$. The third contains only odd modes and is hence symmetric about $\phi = \pi/4$, while the fourth contains only even modes and is antisymmetric about $\phi = \pi/4$. The third and fourth modes have the permutation symmetry mentioned above. These symmetry properties are again the same as found by Scott (2013).

4. Conclusion

In order to use analysis, the flow has been restricted to a trihedral rectangular corner, that is, the first octant bounded by the coordinate planes. With an assumed symmetric dependence on x, y, z, a crucial advantage is achieved by using the three sets of spherical coordinates defined by Gomilko et al. (2003). Solutions are constructed to have zero tangential velocity at all three walls and then symmetrically superposed to eliminate normal flow at any wall. Complex eigenvalues are numerically determined but even integers are eigenvalues with solutions of different structure. Since the latter provide the dominant self-similar flow, trapped eddies cannot occur in a trihedral rectangular corner. In particular, the computed streamlines displayed by Shankar (2007, §12.3) would, with more details of the flow in the bottom corners of the lid-driven cavity flows of various aspect ratios, not exhibit trapped fluid.

References

Davis, A. M. J.: 1983, Force and torque formulae for a sphere moving in an axisymmetric Stokes flow with finite boundaries: asymmetric stokeslets near a hole in a plane wall, *Int. J. Multiphase Flow* **9**, 575–608.

Davis, A. M. J. and O'Neill, M. E.: 1977, Separation in a slow linear shear flow past a cylinder and a plane, *J. Fluid Mech.* **81**, 551–564.

Davis, A. M. J., O'Neill, M. E., Dorrepaal, J. M. and Ranger, K. B.: 1976, Separation from the surface of two equal spheres in Stokes flow, *J. Fluid Mech.* **77**, 625–644.

Dean, W. R. and Montagnon, P. E.: 1949, On the steady motion of a viscous liquid in a corner, *Proc. Camb. Phil. Soc.* **45**, 389–394.

Gomilko, A. M., Malyuga, V. S. and Meleshko, V. V.: 2003, On steady Stokes flow in a trihedral rectangular corner, *J. Fluid Mech.* **476**, 159–177.

Gradshteyn, I. S. and Ryzhik, I. M.: 2000, *Table of Integrals, Series, and Products*, 6 edn, Academic Press, San Diego.

Guglielmini, L., Rusconi, R., Lecuyer, S. and Stone, H. A.: 2011, Three-dimensional features in low-Reynolds number confined corner flows, *J. Fluid Mech.* **668**, 33–57.

Hills, C. P. and Moffatt, H. K.: 2000, Rotary honing: a variant of the Taylor paintscraper problem, *J. Fluid Mech.* **418**, 119–135.

Leriche, E. and Labrosse, G.: 2011, Are there localized eddies in the trihedral corners of the stokes eigenmodes in cubical cavity?, *Computers & Fluids* **43**, 98–101.

Liu, C. H. and Joseph, D. D.: 1978, Stokes flow in conical trenches, *SIAM J. Appl. Math.* **34**, 286–296.

Malhotra, C. P., Weidman, P. D. and Davis, A. M. J.: 2005, Nested toroidal vortices between concentric cones, *J. Fluid Mech.* **522**, 117–139.

Meleshko, V. V.: 1996, Steady Stokes flow in a rectangular cavity, *Proc. R. Soc. Lond.* A **452**, 1999–2022.

Moffatt, H. K.: 1964, Viscous and resistive eddies near a sharp corner, *J. Fluid Mech.* **18**, 1–18.

Mustakis, I. and Kim, S.: 1998, Microhydrodynamics of sharp corners and edges: traction singularities, *AiChE J.* **44**, 1469–1483.

Scott, J. F.: 2013, Moffatt-type flows in a trihedral cone, *J. Fluid Mech.* **725**, 446–461.

Shankar, P. N.: 2007, *Slow Viscous Flow*, Imperial College Press, London.

Shankar, P. N. and Deshpande, M. D.: 2000, Fluid mechanics in the driven cavity, *Ann. Rev. Fluid Mech.* **32**, 93–136.

Sznitman, J., Guglielmini, L., Clifton, D., Scobee, D., Stone, H. and Smits, A. J.: 2012, Experimental characterization of three-dimensional corner flows at low-Reynolds numbers, *J. Fluid Mech.* **707**, 37–52.

Wakiya, S.: 1976, Axisymmetric flow of a viscous fluid near the vertex of a body, *J. Fluid Mech.* **78**, 737–747.